Temperature and Light-Induced Structural Changes in Photosynthetic Reaction Center Proteins Probed by X-ray Absorption Fine Structure

Lin X. Chen,* Lisa M. Utschig, Sandra L. Schlesselman, and David M. Tiede*

Chemistry Division, Argonne National Laboratory, Argonne, Illinois 60439

Received: July 29, 2003; In Final Form: January 14, 2004

Structures of the Fe^{2+} binding site in photosynthetic reaction center (RC) proteins from *Rhodobacter sphaeroides* R26 were obtained by Fe K-edge X-ray absorption fine structure (XAFS) spectroscopy. Measurements were taken at cryogenic and room temperatures, in the dark as well as in the light-induced charge-separated state $P^+Q_AQ_B^-$. Evidence for protein matrix expansion near the Fe^{2+} site because of lowering the temperature from 290 to 15 K was observed as elongation of Fe^{2+} to neighboring atom distances. Upon formation of the charge-separated state $P^+Q_AQ_B^-$, the distances between the Fe^{2+} and neighboring atoms were reduced slightly. Replacing the native Fe^{2+} with either Mn^{2+} or Zn^{2+} resulted in distinct differences in local structural responses to both temperature and charge separation, suggesting that the conformation changes caused by these factors may follow different paths in the potential energy landscape of the protein. The XAFS measurements of Fe^{2+} site structure revealed a more symmetrically oriented imidazole ligands arrangement around Fe than those in current crystal structures. These measurements for high-precision Fe site local structure indicate that XAFS is a useful technique for probing structural changes in the metal site environment because of temperature change, metal replacement, and light-induced charge separation in the reaction center proteins.

Introduction

Primary reactions of solar energy conversion in photosynthetic bacteria are accomplished via light-initiated electron transfer through a series of pigments embedded in reaction center (RC) proteins. The primary electron donor in a photosynthetic bacterial reaction center is a pair of bacteriochlorophylls, the special pair P. An electron is transferred from the photoexcited state of P to a bacteriopheophytin, H_A, within a few picoseconds, then to a quinone cofactor, Q_A, in 150−250 ps. The remarkably small activation energies for these reactions demonstrate the lack of significant structural reorganization upon electron transfer.[1,2] Subsequent electron transfers occur between Q_A and a second quinone, Q_B. Q_B functions as a two-electron, two-proton acceptor following successive turnovers of the RC photochemistry.[3−5] The biphasic $P^+Q_A^-Q_B \rightarrow P^+Q_AQ_B^-$ electron-transfer reaction differs from earlier electron transfers in the RC in that it is a temperature-activated, conformationally gated reaction, believed to be rate-limited by the dynamics of a protein conformational change.[5−8] Resolution of the structural basis for conformational gating in the final electron-transfer steps in the reaction center is central for understanding mechanisms for electron-transfer coupled proton-uptake function.

Crystal structures of the reaction center frozen in the dark and under the light have shown two distinctive sites for Q_B, namely, the distal and the proximal positions.[9,10] The observation of the significant shift in position and rotation of Q_B in the light-adapted structures relative to those in the dark led to the proposal that the proximal and distal Q_B positions correspond to active and inactive conformations with respect to electron transfer from Q_A to Q_B and that movement between these two configurations represents the conformational gate.[9] However, the correlation between the shift in Q_B configuration and rate-limiting conformational change has not been fully established. For example, recent studies with reaction center mutants having Q_B locked predominately in the proximal site[9] continue to show conformationally gated electron transfer.[11] Furthermore, vibrational spectroscopy has demonstrated comparable H-bonding occurs for both Q_A and Q_B and that the H-bonding patterns and quinone interactions within the binding sites do not change upon illumination.[9,12] This spectroscopic data argue against a large-scale, light-induced shift in the position of Q_B as part of the gating mechanism for reaction centers in noncrystalline states.

The strong influence of the reaction center environment on the kinetics of the $P^+Q_A^-Q_B \rightarrow P^+Q_AQ_B^-$ electron transfer raises further questions concerning the correlation between crystallographic conformations and functional rate-limiting steps. Noteworthy is the more than 10-fold slowing of electron transfer upon extraction of the reaction center from the photosynthetic membrane from *Rhodobacter sphaeroides* and *capsulatus*.[13] This indicates that rate limitations under photosynthetic conditions are likely to differ significantly from those in isolated and crystalline states. The complexity of the conformational landscape linked to the $P^+Q_A^-Q_B \rightarrow P^+Q_AQ_B^-$ electron transfer in the isolated state is also demonstrated by the pH and temperature dependencies of the reaction[14−16] and by the sensitivity of the reaction rate to a large range of experimental conditions.[5] Molecular modeling and spectroscopic experiments[17] have identified multiple types of atomic reorganization in addition to the shifts in quinone position that potentially could have significant impact on the energetics of $P^+Q_A^-Q_B \rightarrow P^+Q_AQ_B^-$ electron transfer. These include proton displacements that potentially lie beyond the resolution of most crystallographic studies.

* Correspondence should be addressed to this author. E-mail: lchen@anl.gov.

10.1021/jp036220r CCC: $27.50
Published on Web 03/02/2004

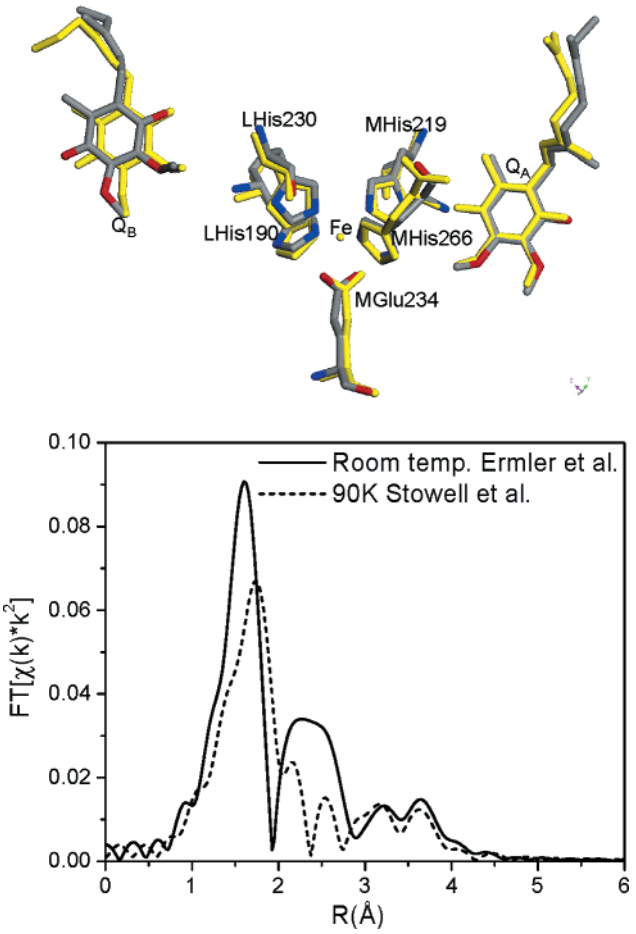

Figure 1. (A) Fe site structure of *Rb. Sphaeroides* reaction center protein at room temperature from Ermler et al. (1*pcr*)[43] and from Stowell et al. (1*aij*)[9] (yellow); (B) Fe K-edge Fourier transformed XAFS spectra from the two structures around the Fe site.

We have initiated a project that examines details in the local structures of the nonheme Fe^{2+} site located between Q_A and Q_B via Fe K-edge X-ray absorption fine-structure (XAFS) spectroscopy.[18−20] XAFS is a sensitive probe of the coordination environment of metal atoms[21−23] that complements X-ray crystallographic structural determination by providing a measure of local structure around metal sites with a resolution far better than what can be achieved with protein X-ray crystallography alone.[24−31] Hence, local structural changes smaller than the precision achieved by protein X-ray diffraction method can be detected. Such high-precision local structures may provide new insights into conformational changes associated with the photo-induced charge separation near or at the Fe^{2+} site of the RC protein.

The Fe^{2+} site is buried in the interior of the RC and situated in the middle of a putative electron-transfer path from Q_A to Q_B. Crystallographic studies have shown that the Fe^{2+} in the bacterial photosynthetic RC is ligated with four nitrogen atoms (N_ϵ) from four different histidine (His) residues and two oxygen atoms of a carboxylate group from a glutamic acid (Glu) residue.[32−35] Two of the four His residues are adjacent to Q_A and Q_B, and at least one of the His residues forms a H-bond with an oxygen atom from Q_A in the dark and light-adapted structures,[9,10] developing the Fe−His-quinone "wire" (see Figure 1). Thus, the Fe^{2+} ion, although it is not directly bound to Q_A or Q_B, may serve as a structural probe for the detailed atomic arrangement in the region connecting Q_A and Q_B sites.

In this report, we have characterized responses of the RC Fe^{2+} site structure to cryogenic cooling in the neutral (PQ_AQ_B) and the charge-separated ($P^+Q_AQ_B^-$) states. These results are relevant to an understanding of the unusual acceleration in $P^+Q_A^-$ charge recombination rate that occurs upon cooling to cryogenic temperatures[36] and to the resolution of the structural reorganization that accompanies $P^+Q_AQ_B^-$ charge separation.[9] In this study, we take advantage of much higher precision structural data for the metal site obtained from XAFS measurements to probe the fine structural changes in the protein matrix surrounding the metal site because of temperature and light-induced charge separation. In addition, the XAFS measurements were conducted on Fe^{2+}-removed, Mn^{2+}- and Zn^{2+}-replaced RCs. These measurements provide insight into the role of the metal ion in determining structure in the metal binding site region.

Materials and Methods

1. Sample Preparation. The carotenoidless photosynthetic mutant *Rb. sphaeroides* R-26 was grown under illumination on both Hunter's medium and Mn-depleted Hunter's media. RCs from this bacterium were isolated as previously described.[37] We have observed >50% incorporation of Mn into the Fe site when the bacterium in grown with the "normal" Hunter's medium containing 6×10^{-6} M $MnSO_4$ and 2.5×10^{-5} M $FeSO_4$.[37] We refer to these RCs with biosynthetically incorporated Mn in the Fe site as Mn^{2+-}RCs. Total exclusion of Mn from the medium results in RCs containing >90% Fe in the Fe site.[38] Fe-removed/Zn-replaced RCs (Zn^{2+-}RC thereafter) were prepared according to the procedure of Utschig.[37] Protein concentrations were determined with the extinction coefficient $\epsilon_{802} = 288\ mM^{-1}\ cm^{-1}$.[39] The amount of Fe, Mn, and Zn bound to the RC was determined using inductively coupled plasma-atomic emission spectroscopy (ICP-AES) on a Thermo Jarell Ash Atomscan Advantage spectrometer.

Q_B was reconstituted by adding quinone (~10 equiv/RC) from a stock solution containing 3.3 mM $ubiquinone_{10}$ (Sigma) and 1.9% LDAO that had been heated to 65 °C for approximately 5 min. DMPC lipid, dimyristoyl L-α-phosphatidylcholine (Sigma), was added in a ratio of 100 lipid/RC. To remove the detergent, the RC−lipid solution was dialyzed at 4 °C into detergent-free buffer containing 10 mM Tris-Cl pH 8.06 and 10 mM NaCl. Following 48 h of dialysis, precipitated RC−lipid complexes were collected by ultracentrifugation.

2. XAFS Measurements and Data Analysis. K-edge XAFS spectra for Mn^{2+-}, Fe^{2+-}, and Zn^{2+-}RCs were collected at beamline 12 BM, Advanced Photon Source of Argonne National Laboratory. Si 111 crystals were used in the monochromator. A Pt-coated mirror was used to focus the beam and to remove higher harmonic X-ray photons. The beam size at the sample was about 0.4 mm (v) × 1 mm (h). A feedback system was used to control the monochromator crystal angle and was set to 70% detuning. A nine-element germanium solid-state detector (Canberra) was used to collect K_α X-ray fluorescence signals from the RC samples with the metal ion concentration of ~2×10^{-4} M. A chromium-, manganese-, or copper-filter was placed in front of the detector for attenuation of elastic scatterings, respectively, for K-edge XAFS measurements of Mn, Fe, and Zn, which increased the relative signal ratio between the metal K_α fluorescence of the RC samples and the elastic scattering from <1:100 to ~1:1. The outputs from the amplifiers of the detector were connected to a group of single-channel analyzers (SCA) with proper upper and lower thresholds to allow only $K_{\alpha1}$ and $K_{\alpha2}$ fluorescence signals of the specific

metal ions to be further processed. An ion chamber was placed before the sample for the X-ray flux reference signal I_0, and the second and the third ion chambers were placed after the sample. A metal foil of the same element as the RC sample inserted between the second and the third ion chambers was used for X-ray photon energy calibration. The output signals from the SCAs were connected to a scaler array which interfaced with a computer hosting a data acquisition program.[40]

Each RC sample in lipid paste was carefully spread to form a thin 2×2 mm^2 film on a sapphire disk and was covered by a polycarbonate film with 5-μm thickness. The sapphire disk was mounted on a copper sample holder attached to a cryogenic system. A Janis cryogenic system with Kapton and quartz windows was used for low-temperature experiments. A xenon lamp (Fisher Scientific) was used to illuminate the sample with an optical fiber bundle through the quartz window of the cryostat. Before each measurement, the sample was kept in the dark for at least 10 min. For experiments with light illumination at cryogenic temperature, the sample was cooled first in dark, then was illuminated for about 10 min before XAFS measurements. After the measurements, the sample was warmed and another XAFS spectrum was taken to check the integrity of the sample. For experiments with light illumination while cooling from 290 K, the light was on until the sample was cooled to the final cryogenic temperature. The sample integrity was also checked after the measurements.

Conventional XAFS data analysis programs, WinXAS (T. Ressler) and FEFF8 (University of Washington), were used in data analysis and simulation of the XAFS spectra of the RCs. Three metal oxalate dihydrate compounds, $FeC_2O_4 \cdot 2H_2O$, $MnC_2O_4 \cdot 2H_2O$, and $ZnC_2O_4 \cdot 2H_2O$ with known crystal structures[41,42] were used as references for structural parameters and the FEFF calculations. Similarly, the Fe^{2+} site XAFS spectra from different crystal structures of the RC were also calculated using FEFF8. Selected single-scattering paths were used to extract the amplitude and the phase parameters of O and N backscatterings for the nearest neighbors, and those parameters were used in subsequent fittings to the equation $\chi(k) = \sum F_i(k) S_0^2(k) N_i/(kR_i^2)\exp(-2\sigma_i^2k^2)\sin[2kR_i + \delta_i(k)]$ (where $F(k)$ is the magnitude of the backscattering; S_0, amplitude reduction factor; N, the coordination number; R, the average distance; σ, the Debye−Waller factor; and δ, the phase shift; the subscript indicates ith atom; k is the electron wavevector). The Fe−N bond lengths obtained from the fits using the parameters from the Fe−N single-scattering paths in the Fe^{2+} site of the RC and from the Fe−O single-scattering path in iron oxalate dihydrate differ only by 0.01 Å. Therefore, we used the single-scattering paths of Fe−O, Mn−O, and Zn−O in corresponding oxalate dihydrate crystal structures to approximate all the metal to the nearest neighbor bonds with both one- and two-distance models. Parameters from the FEFF calculations were first fit to the experimental spectra of metal oxalate dihydrates. Agreements for the first shell bond distances were within 0.02 Å for all the reference compounds. Systematic corrections were made according to the results of the fits for metal oxalate dehydrates with known crystal structures. The observed bond distance differences at different temperatures and between the neutral and the charge separation states of RC samples are conserved regardless the method used to extract the amplitude and the phase parameters. The k ranges for the Fourier transform were nearly the same for all RC samples and specified in the corresponding figure captions, and 2% Hanning window was applied. In accord with the crystal structure of the RC, the coordination number of the metal ion was fixed to six in one-distance model for the nearest neighbors and was divided into fixed values of four and two, respectively, to depict the four N and two O ligands in two-distance model. This procedure is based on an assumption that the diversity of the bond distances is within the same RC protein molecule, rather than among different protein molecules. The validity of this assumption will be discussed below. Because of the interference between the first and the second peaks in the FT-XAFS spectra of Fe^{2+}−RC samples, the R range for back Fourier transform included both peaks and the fittings were performed simultaneously for the nearest and next nearest neighboring atomic shells. The FT-XAFS spectra for Mn^{2+}− and Zn^{2+}−RC did not show significant interference between the two peaks and the second peak amplitudes were small, so the back Fourier transforms were performed on first peak only, and the structural parameters for the nearest neighboring shell were extracted.

To simulate an XAFS spectrum for the Fe site in the RC protein which resembles the experimental data, the His ligand orientations around the Fe site were adjusted using Material Studio software (Accelyrs Inc.). Subsequently, the XAFS spectrum of modified structure was calculated with FEFF8 and compared with the experimental data.

Results

1. Temperature-Induced Structural Change in the Metal Binding Site. Crystal structures for wild-type RCs from *Rb. sphaeroides* are 2.65 Å resolution at room temperature[43] and 2.20 Å resolution at 77 K[9] (1*pcr* and 1*aij* from the Protein Data Bank, http://www.rcsb.org/pdb/). These data provide the opportunity to search for possible temperature dependence in the RC structure. While the two structures are globally similar, they are locally different around the Fe^{2+} site (Figure 1A), particularly in the positions of LHis190 and MHis266. It is rather difficult to evaluate the relevancy of these variations because the two structures have been independently refined with different experimental resolution. Nevertheless, subtle differences cannot be expected to be accurately distinguished within experimental crystallographic resolution. In contrast, the corresponding Fourier transformed (FT) XAFS spectra for these structures (Figure 1B) differ not only in nearest neighbor distances, but also in the distant atoms. These results clearly demonstrate the high precision of the XAFS technique and the opportunity to utilize XAFS data for testing or accurately refining the crystallographic Fe^{2+} site structures.

Experimental Fe K-edge XAFS spectra of the Fe^{2+} site in *Rb. sphaeroides* RC at 290 and 15 K are shown in Figure 2. The low-temperature XAFS spectrum has higher amplitudes of oscillations because of reduced Debye−Waller factors (Figure 2A and 2B). The FT-XAFS spectra at both temperatures clearly show three peaks at $R = 1-2$ Å, 2−3 Å, and 3−4 Å, corresponding to three or more neighboring shells of atoms around Fe^{2+} site (Figure 2B, without phase correction). The positions of these peaks are temperature dependent, with longer average neighbor distances from the Fe^{2+} at 15 K. The temperature dependence of the distances from the Fe^{2+} to the first two nearest neighboring shells is depicted by Figure 2C showing isolated XAFS spectra for the first two peaks along with the fitting functions. At 290 K, Fe^{2+} FT-XAFS spectrum closely agrees with earlier studies on *Rb. sphaeroides* RCs, which also displays almost identical oscillatory pattern as well as the three-peak features in Fourier transformed spectra.[18,19] Obviously, the experimental XAFS spectra in Figure 2 clearly deviate from those calculated using crystal structures in Figure 1B.

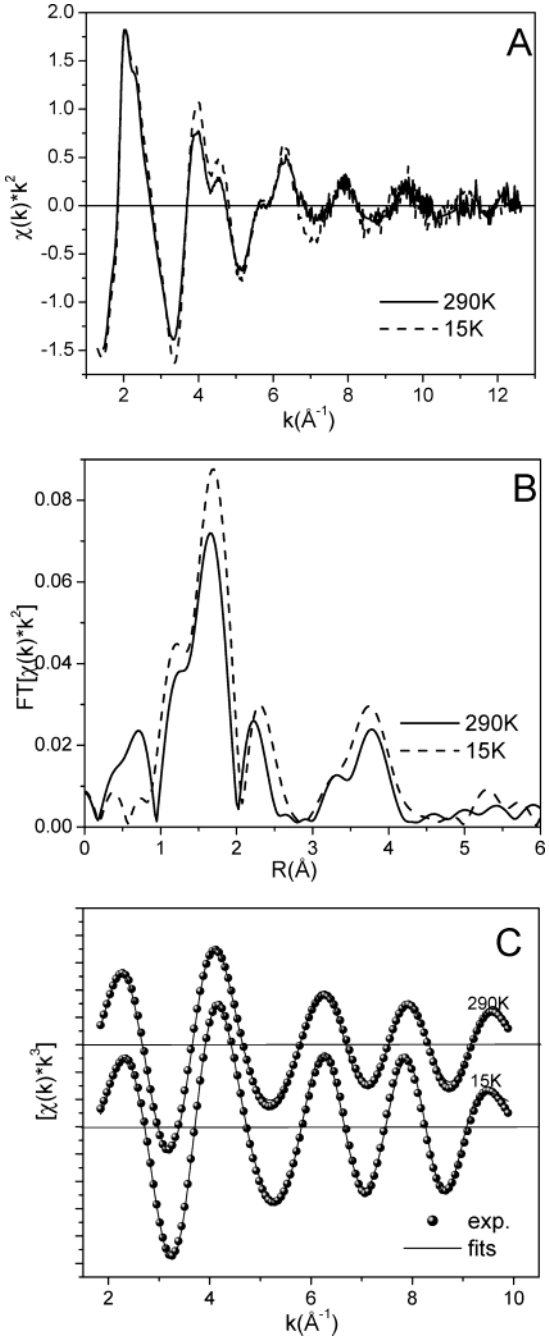

Figure 2. Fe K-edge XAFS spectra of *Rb. Sphaeroides* R26 at different temperatures, (A) k^2-weighted XAFS spectra (the deglitching was performed at $k = 8.5$ and 10.5 Å^{-1} for 290 K data); (B) k^3 weighted FT-XAFS spectra (transformed from $k = 1.8-10.2$ Å^{-1}); (C) back-transformed XAFS spectra ($R = 1.0-2.8$ Å) for the first two peaks with fitting functions that uses two-distance model for the nearest neighbors.

The first shell XAFS peak originates from the distance between the metal ion to its ligands including four N_ϵ atoms from imidazole groups of LHis190, LHis230, MHis219, MHis266, and two $O_{\delta 1,\delta 2}$ atoms from MGlu234. Because Figure 2B indicates the interference between the first and the second peaks in the FT-XAFS spectra, the data analysis was carried out by fitting the XAFS spectra of isolated first and second peaks together. The one-distance model for the nearest neighbors resulted in poor fits of average distances of 2.07 and 2.11 Å for the Fe−N(O) bonds at 290 and 15 K, respectively (Table 1). The two-distance model with coordination numbers of 4 and 2 for the nearest neighbors improved the fits significantly, Fe−N(O) distances of 2.09 and 1.88 Å, respectively, at 290 K, and of 2.14 and 1.91 Å, respectively, at 15 K (Table 1). The residuals of the fits clearly favor the two-distance model for the nearest neighbor distance (Figure 2C and Table 1), which is more visible in the $k > 8$ Å^{-1} region. Because transition-metal ions bind imidazole N_ϵ atoms and carboxylate O_δ atoms via different molecular orbitals,[44] the most likely division in the coordination number of the metal ion in the two-distance model is 4 (Fe−N) and 2 (Fe−O) (Table 1), although other kinds of divisions are also possible. To retain self-consistency of the fits, the coordination numbers were fixed to the same values during the fitting. Because of the uncertainty in the coordination number division, these results should be viewed with caution.

The second nearest neighbor peak in Figure 2B appears between 2 and 3 Å (without phase correction) and arises from both single and multiple scatterings because of atoms located in distances of 2.5−3.3 Å from Fe. This peak also shifts to a longer distance at 15 K compared to at room temperature. The next nearest neighboring shell of Fe^{2+} was modeled by the second shell atoms from Fe^{2+} in oxalate dehydrate which has an average distance of 2.89 Å. Because of the disorder of the second nearest neighbors, we only expect an average value of the distance for the next nearest neighbor distances to be extracted, which result in the values of 2.87 and 2.90 Å, respectively, for 290 and 15 K data. Therefore, on average, the expansion of the nearest and next nearest neighbor distances from Fe^{2+} because of lowering temperature to 15 K is 0.03−0.04 Å. Both atomic shells expand to longer distance from the Fe^{2+}.

Figure 2B also shows a prominent third peak near 3.8 Å (without phase correction). This peak was also observed in previous studies and was attributed to the distant atoms about 4.3 Å away from the Fe[18,19] but was not predicted with this magnitude from calculations on the basis of the crystal coordinates (Figure 1B). The shapes and amplitudes of both the second and third shell XAFS peaks are attributed to the multiple scatterings resulted from imidazole rings of His residues and are sensitive to the relative angular orientations of these ligands. Since the RC quinones make hydrogen-bonding contacts to coordinating His ligands,[9] the second and third shell XAFS peaks potentially provide a sensitive reporter of conformational changes in the quinone binding regions.

In contrast to the expansion detected in the Fe^{2+} site structure upon cooling to 15 K, a smaller temperature effect for the Mn^{2+} site was observed in Mn^{2+}−RCs (Figure 3 and Table 2). The first shell Mn−N(O) distances at 290 and 25 K differ by only 0.01 Å from one-distance model and 0.02 Å from two-distance model. The two-distance model only moderately reduces residuals of the fits (less than a factor of 2), implying that a one-distance model may be adequate. Therefore, the Mn−N(O) bond distances are less diverse compared to the Fe−N(O) bonds in the RC. In addition, unlike the Fe^{2+} FT-XAFS, the 290 and 25 K Mn^{2+} FT-XAFS do not resolve into clear second and third shell peaks. This suggests that the Mn^{2+} incorporation induces a reorganization of the ligand structure.

The significant temperature effect was also observed in Zn^{2+}−RCs. The fits of the first peak in Figure 4B are significantly worse with one-distance model compared to Fe^{2+}− and Mn^{2+}−RCs and are improved substantially with two-distance model. The two distances increase by 0.01 and 0.04 Å, respectively, at 14 K compared to at room temperature (Table 3). On the other hand, the averaged nearest neighbor distances at 290 and 14 K only differ by 0.02 Å. Substantial changes in the second and third peaks were also observed in

TABLE 1: Structure Parameters for the Neighbors of Fe^{2+} in Photosynthetic Bacterial Reaction Center Protein from *Rb. Sphaeroides* R26[a]

condition	shell[b]	N	R (Å)	R_{avg} (Å)[c]	σ^2 (Å^2)	residuals
dark, 290 K	1	6.0 ± 1.0	2.08 ± 0.02		0.01	20
	2	9.0 ± 2.0	2.85 ± 0.02		0.02	
	1	4.0 ± 0.8	2.09 ± 0.02	2.02	0.002	8
		2.0 ± 0.5	1.88 ± 0.02		0.005	
	2	9.0 ± 2	2.87 ± 0.02		0.02	
dark, 15 K	1	6.0 ± 1.0	2.11 ± 0.02		0.01	23
	2	9.0 ± 2.0	2.88 ± 0.02		0.02	
	1	4.0 ± 0.8	2.14 ± 0.02	2.06	0.005	11
		2.0 ± 0.5	1.91 ± 0.02		0.01	
	2	9.0 ± 2.0	2.90 ± 0.02		0.01	
15 K then light	1	6.0 ± 1.0	2.09 ± 0.02		0.01	21
	2	9.0 ± 2.0	2.88 ± 0.02		0.02	
	1	4.0 ± 0.8	2.12 ± 0.02	2.06	0.007	9
		2.0 ± 0.5	1.93 ± 0.02		0.01	
	2	9.0 ± 2.0	2.87 ± 0.02		0.02	
light while cool to 15 K	1	6.0 ± 1.0	2.06 ± 0.02		0.01	10
	2	6.0 ± 2.0	2.87 ± 0.02		0.02	
	1	4.0 ± 1.0	2.08 ± 0.02	2.02	0.01	8
		2.0 ± 1.0	1.92 ± 0.02		0.003	
	2	4.0 ± 1.0	2.90 ± 0.02		0.01	

[a] Using Fe^{2+} oxalate dihydrate as the reference.[51,52] The structural parameters were extracted from calculate spectrum by FEFF7.0. [b] Shell is the index for neighboring atomic shells. Shell = 1 is for the nearest neighbors, 2, is for the next nearest neighbors, etc. [c] Only applicable to the nearest neighbors with the two-distance model, defined as $\sum n_j R_j / \sum n_j$, where $n_1 = 4$ and $n_2 = 2$ for the nearest neighbors.

TABLE 2: Structure Parameters for the Nearest Neighbors of Mn^{2+} in Modified Photosynthetic Bacterial Reaction Center Protein from *Rb. Sphaeroides* R26[a]

condition	N	R (Å)	R_{avg} (Å)[b]	σ^2 (Å^2)	residuals
dark, 290 K, 1-distance	6.0 ± 1.0	2.19 ± 0.02		0.02	14
dark, 290 K, 2-distance	4.0 ± 1.0	2.24 ± 0.02	2.18	0.008	8
	2.0 ± 0.5	2.07 ± 0.02		0.01	
dark, 25 K, 1-distance	6.0 ± 1.0	2.20 ± 0.02		0.01	18
dark, 25 K, 2-distance	4.0 ± 1.0	2.25 ± 0.02	2.20	0.006	10
	2.0 ± 1.0	2.11 ± 0.02		0.002	
25 K then light, 1-distance	6.0 ± 1.0	2.19 ± 0.02		0.02	13
25 K then light, 2-distance	4.0 ± 1.0	2.23 ± 0.02	2.18	0.01	10
	2.0 ± 1.0	2.09 ± 0.02		0.01	
light while cool to 25 K, 1-distance	6.0 ± 1.0	2.15 ± 0.02		0.02	21
light while cool to 25 K, 2-distance	4.0 ± 1.0	2.17 ± 0.02	2.12	0.01	5
	2.0 ± 1.0	2.01 ± 0.02		0.02	

[a] Using Mn^{2+} oxalate dihydrate as the reference.[51,52] The structural parameters were extracted from calculate spectrum by FEFF7.0. [b] Only for the two-distance model, defined as $\sum n_j R_j / \sum n_j$, where $n_1 = 4$ and $n_2 = 2$ for the nearest neighbors.

Figure 4B, indicating that structural change was associated with not only a minor expansion of the surrounding protein matrix, but also the reorientation of the ligands at cryogenic temperature.

2. Light-Induced Structural Changes in the Metal Binding Site. Fe^{2+}-site XAFS spectra of RC were measured under three experimental conditions: Condition A, cooling to 15 K in the dark; B, cooling to 15 K in the dark then illuminating for 10 min or continuously; and C, cooling to 15 K under illumination. Previous studies have shown that cooling dark-adapted RCs to cryogenic temperatures traps RCs in a configuration where light-induced electron transfer from Q_A^- to Q_B is prevented, while cooling RCs in the light traps a charge-separated adapted configuration that allows light-induced $P^+Q_AQ_B^-$ formation to occur at cryogenic temperatures.[36] Furthermore, we have observed with EPR spectroscopy that comparable $P^+Q_AQ_B^-$ adapted configurations can be trapped by cooling while flashed with 1 Hz laser excitation from room temperature to 20 K with Zn^{2+}−RC as well as Mn^{2+}−RCs.[45] Therefore, the XAFS spectra under conditions A and C depict Fe^{2+} site structures trapped in the dark-adapted PQ_AQ_B and light-adapted $P^+Q_AQ_B^-$ states, respectively, while condition B provides a measure of structural reorganization induced following $P^+Q_A^-Q_B$ formation at low temperature.

Overall, experimental XAFS spectra recorded for Fe^{2+}−RCs under each of these conditions were quite similar, as shown in Figure 5. XAFS spectra recorded under conditions A, dark-adapted, and B, low-temperature light-adapted, were nearly indistinguishable, whereas those recorded under condition C, the $P^+Q_AQ_B^-$ adapted state, showed small, but resolvable differences. Given the sensitivity of XAFS to structural change, these results demonstrate that the main features of the Fe^{2+} site structure are preserved in each of these conditions and that only subtle changes are induced by charge separation.

The subtle structural adaptations of the Fe^{2+} in response to $P^+Q_AQ_B^-$ formation are illustrated by the XAFS spectra shown in Figure 5. Fitting the first peak that corresponds to the first shell Fe−N(O) bonds with one-distance model seems to be adequate, because the two-distance model only improves the fit slightly (Table 1). Compared to the dark-adapted RC with PQ_AQ_B state at 15 K, the average Fe^{2+}−N(O) bond length is shortened by 0.04 Å upon the $P^+Q_AQ_B^-$ formation. Meanwhile, the third shell peak between $R = 3-4$ Å (without the phase correction) in the $P^+Q_AQ_B^-$ state also shifts to a smaller distance compared to that in the PQ_AQ_B state.

In contrast, the Fe site structure following low-temperature $P^+Q_A^-Q_B$ formation shows no change in average Fe−N distance and only slight shortening within the experimental error in the

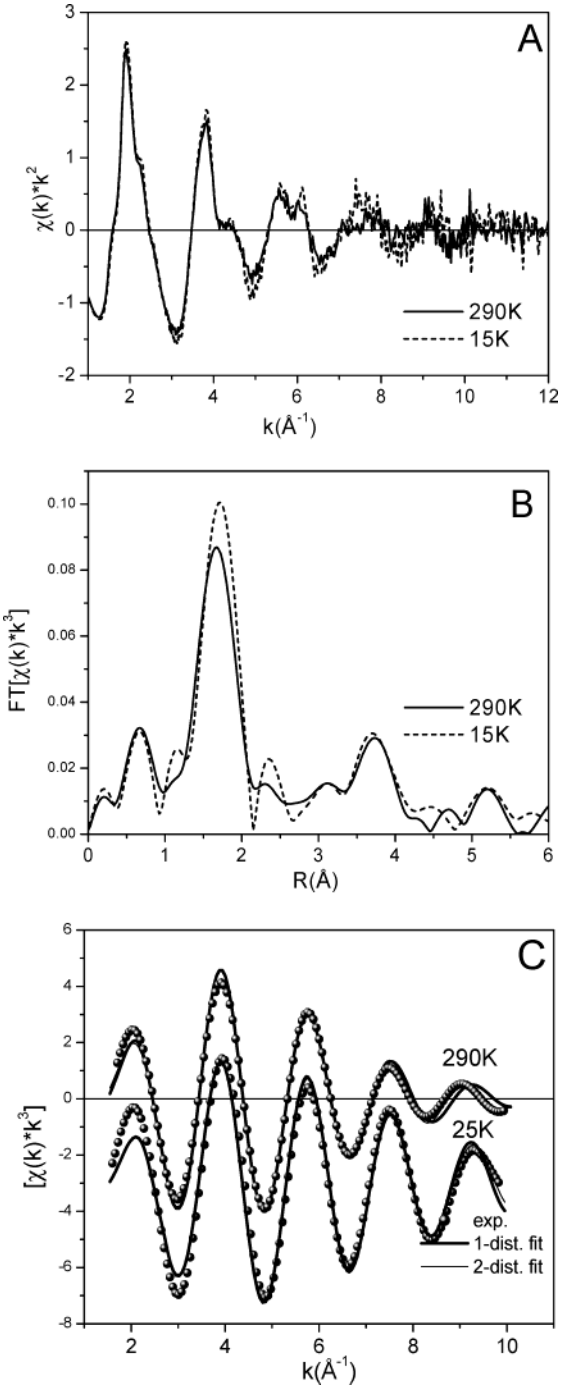

Figure 3. Mn K-edge XAFS spectra of *Rb. Sphaeroides* Mn^{2+}−RC at different temperatures, (A) k^2-weighted XAFS spectra; (B) k^3 weighted FT-XAFS spectra (transformed from $k = 1.7-10.1$ Å^{-1}); (C) back-transformed XAFS spectra ($R = 1.02-2.15$ Å) for the first peak with fitting functions with one- and two-distance models.

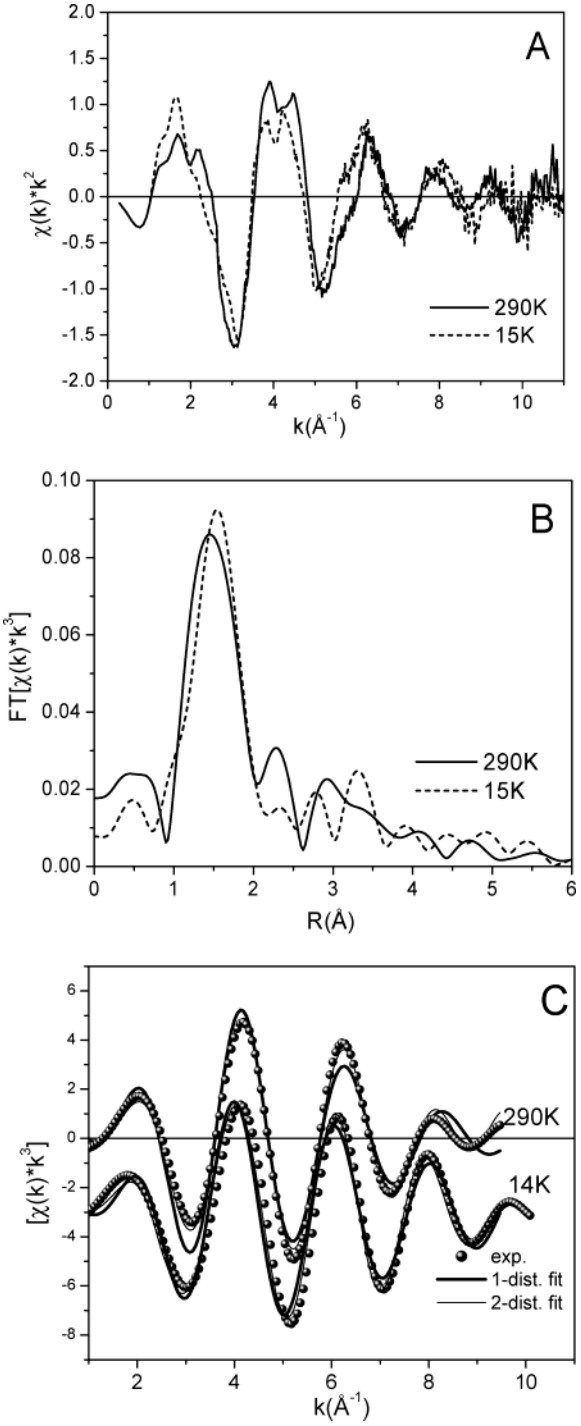

Figure 4. Zn K-edge XAFS spectra of *Rb. Sphaeroides* Zn^{2+}−RC at different temperatures (A) k^2-weighted XAFS spectra; (B) FT-XAFS spectra (transformed from $k = 1.7-10.1$ Å^{-1}); (C) back-transformed XAFS spectra ($R = 1.02-2.15$ Å) for the first peak with fitting functions with one- and two-distance models.

average Fe−O distance (Table 1). This result demonstrates the lack of significant structural adaptation of the Fe^{2+} site in response to formation of the $P^+Q_A^-Q_B$ at low temperature.

Remarkably, the structure for the $P^+Q_AQ_B^-$ adapted state at 15 K, where low-temperature $P^+Q_A^-Q_B \rightarrow P^+Q_AQ_B^-$ is enabled, resembles that of PQ_AQ_B state at 290 K, whereas it differs more significantly from the Fe^{2+} site structure for the inactive dark-adapted low-temperature structure. These structural changes, although subtle, reflect changes in the forces acting on the Fe^{2+} coordination environment and may be related to conformational differences in protein that limit electron transfer from Q_A^- to Q_B at low temperature.

Comparable room temperature[8,46] and temperature-dependent[8,46] $P^+Q_A^-Q_B \rightarrow P^+Q_AQ_B^-$ electron-transfer processes occur in native, Mn^{2+}−RCs as well as Zn^{2+}−RCs. The changes in XAFS spectra for the Mn^{2+}−RCs in response to light-induced charge separation are shown in Figure 6. The average nearest neighbor distance from Mn^{2+} with two-distance fits is 0.08 Å shorter in $P^+Q_AQ_B^-$ adapted state compared to the dark-adapted PQ_AQ_B state (Table 2). In addition, the third shell peak also moves to shorter distances in response to $P^+Q_AQ_B^-$ charge separation. A very small change in the Mn^{2+} site structure was seen upon prolonged $P^+Q_A^-Q_B$ formation at 25 K. This pattern

TABLE 3: Structure Parameters for the Nearest Neighbors of Zn^{2+} in Modified Photosynthetic Bacterial Reaction Center Protein from *Rb. Sphaeroides* R26[a]

condition	N	R (Å)	R_{avg} (Å)[b]	σ^2 (Å^2)	residuals
dark, 290 K, 1-distance	6.0 ± 1.0	1.95 ± 0.02		0.01	26
dark, 290 K, 2-distance	4.0 ± 1.0	2.02 ± 0.02	1.96	0.0002	7
	2.0 ± 0.5	1.84 ± 0.04		0.003	
dark, 14 K, 1-distance	6.0 ± 1.0	1.99 ± 0.02		0.007	25
dark, 14 K, 2-distance	4.0 ± 1.0	2.03 ± 0.02	1.98	0.002	6
	2.0 ± 0.5	1.88 ± 0.04		0.002	
14 K then light, 1-distance	6.0 ± 1.0	2.01 ± 0.02		0.01	20
14 K then light, 2-distance	4.0 ± 1.0	2.05 ± 0.02	1.99	0.006	9
	2.0 ± 0.5	1.89 ± 0.04		0.008	
	2.0 ± 0.5				
light while cool to 14 K, 1-distance	6.0 ± 1.0	2.00 ± 0.02		0.01	37
light while cool to 14 K, 2-distance	4.0 ± 1.0	2.07 ± 0.02	2.01	0.003	17
	2.0 ± 1.0	1.90 ± 0.04		0.0004	

[a] Using Zn^{2+} oxalate dihydrate as the reference.[51,52] The structural parameters were extracted from calculate spectrum by FEFF7.0. [b] Only for the two-distance model, defined as $\sum n_j R_j / \sum n_j$, where $n_1 = 4$ and $n_2 = 2$ for the nearest neighbors.

of structural response of the Mn^{2+} coordination environment to charge separation is closely analogous to that of the native Fe^{2+} coordination environment.

Compared to the Fe^{2+} and Mn^{2+} sites structures, the Zn^{2+} in the iron-quinone site showed more visible spectral change in response to the charge separation as shown in Figure 7A. However, the actual average nearest distance to the Zn^{2+} site shown in Table 3 indicates a slight increase of 0.03 Å in the average nearest neighbor distance at the $P^+Q_AQ_B^-$ state. Compared to FT-XAFS spectra for Fe−RC and Mn^{2+}−RC where three peaks are clearly shown (Figures 6 and 7), FT-XAFS spectra of Zn^{2+}−RC do not have clearly defined second and third peaks, but a cluster of peaks. This is an indication of a very different coordination environment for the Zn^{2+} site from those of Fe^{2+} and Mn^{2+} sites, where structural changes caused by the formation of $P^+Q_AQ_B^-$ may involve reorientation of the ligands as well as the variation in the coordination geometry.

Discussion

The Reaction Center Fe^{2+} Site Structure. XAFS is a direct structural technique that complements X-ray crystallography analysis by providing the opportunity to resolve metal ion coordination site structures in noncrystalline materials with a precision typically much higher than that achieved by crystallography alone. Distinctly different spectral features of the Fe^{2+} site in the RC (Figure 1B) revealed by the XAFS from two globally identical structures from X-ray diffraction studies[9,43] suggest the potential for determining subtle structural changes. A precise characterization of the RC of the Fe^{2+} coordination environment is important because metal coordination environments in proteins frequently differ from those of small metal coordination compounds as a result of the interplay between metal−ligand electronic interactions and the covalent linkage of the ligands with the surrounding protein matrix. Because of this interplay, proteins can adapt unusual metal coordination geometries that are not necessarily found in small metal complexes.[47]

The third peak at $R = 3.5-4.0$ Å in FT-XAFS spectra (Figure 2B, without phase correction) originates from multiple scatterings from the imidazole rings of His groups, in particular, N_δ and C_γ atoms. The relatively high intensity of this peak in the RC, however, reflects the reduced Debye−Waller factors of distant atoms because of the restriction of the surrounding protein matrix on the thermal motions of the ligands. Such a restriction is absent for metal complexes with similar monodentate ligands in solution at room temperature, which rarely display such high-intensity peaks at the same distance because of large Debye−Waller factors for distant atoms from the metal due to ligand thermal motions and solvent molecule stochastic collisions. Therefore, the high intensity of the third peak in FT-XAFS spectra of Fe site in the RC reflects the rigidity of the metal site imposed by the protein matrix, which, on the other hand, enhances communications between metal sites with their neighbors. Hence, the unique characteristics of the distant peaks in FT-XAFS spectra of the metal site in protein also validate the use of XAFS spectra to probe structural changes of distant neighbors.

Although there is no known major and definite role of the Fe^{2+} site in the electron transfer from Q_A to Q_B, the removal of the Fe^{2+} caused significant change in the rate of the electron transfer.[37,48,49] Therefore, the possible function of the Fe^{2+} site is to keep the tertiary structural integrity of the RC protein.[46] Consequently, any structural changes that may alter the protein integrity can be "felt" by the Fe^{2+} site, and the local structures of the site measured by XAFS is likely sensitive to the protein structural changes that may affect electron transfer, especially the electron transfer from Q_A to Q_B that takes place in its vicinity. Our results from XAFS spectra of the Fe^{2+} site have indeed shown structural changes in response to the temperature change, the charge separation, and the replacement of the divalent metal ion. In particular, the distant atomic shells from the Fe^{2+} site, located around 3−4 Å, are sensitive to the orientation relative to the Fe−N or Fe−O bonds, where they can potentially provide structural information with a sphere centered at Fe^{2+} with a radius up to 4 Å.

However, because XAFS measures the signals from all metal sites of the same kind, this technique is unable to distinguish whether the heterogeneity of the bond distances is from each identical protein molecule or from different molecules. We assumed in our XAFS data analysis that the two distances for the metal sites were from the same molecule and all molecules had the identical metal binding site structure. However, we cannot rule out the structural heterogeneity among different RC molecules as well as diverse distances in the inner coordination sphere of the metal ion. Nevertheless, the XAFS spectra positively identified the metal−ligand bond expansion at cryogenic temperature compared to that at room temperature rather than the mere reduction of the Debye−Waller factors as observed in simple metal coordination compounds.[50] In addition, our study also identified the changes around the metal sites upon photoinduced charge separation $P^+Q_AQ_B^-$, although the metal sites were not involved in the electron transfer and any redox process. Hence, these changes reflected the structural changes in the surrounding protein. Thus, the metal site XAFS spectra

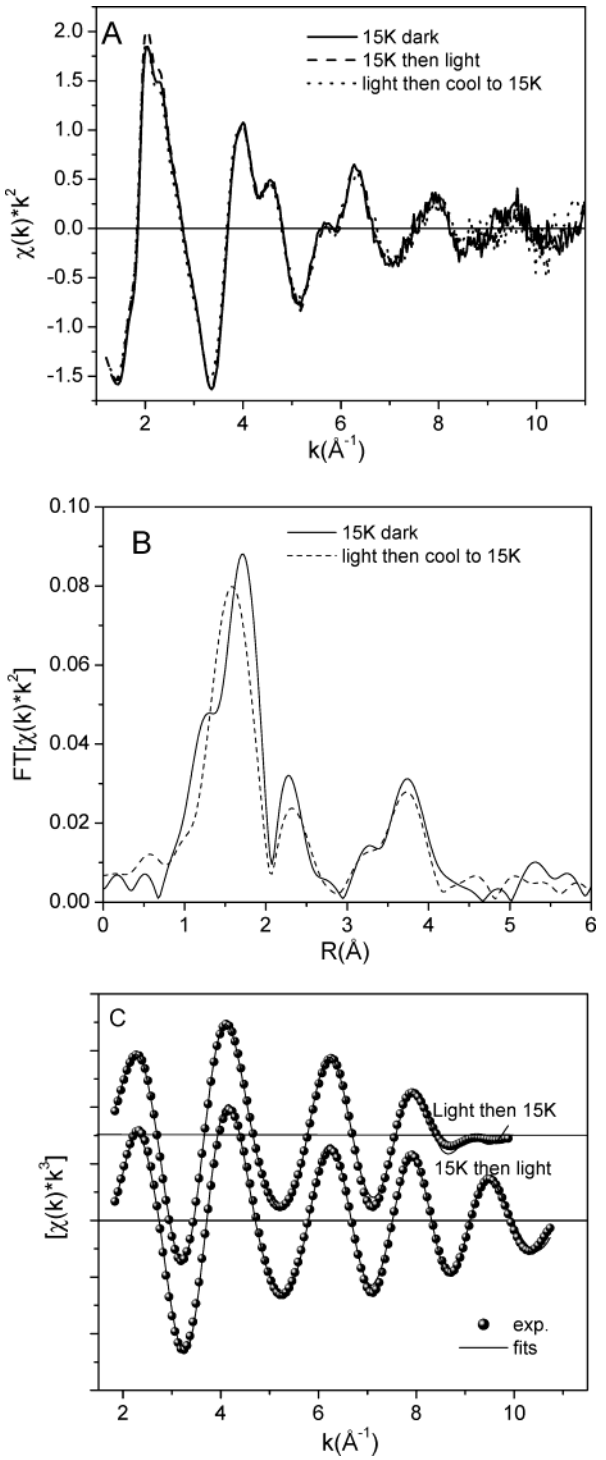

Figure 5. Fe K-edge XAFS spectra for Fe^{2+} site in *Rb. Sphaeroides* R26 RC in neutral state PQ_AQ_B and charge separate state $P^+Q_AQ_B^-$ at 15 K. (A) k^2-weighted XAFS spectra, (B) Fourier transformed XAFS spectra (transformed from $k = 1.8-10.1$ Å^{-1}), and (C) back-transformed XAFS spectra ($R = 0.8-2.8$ Å) for the first two peaks for $P^+Q_AQ_B^-$ (light then 15 K) and $P^+Q_A^-Q_B$ (15 K then light) with fitting functions that uses two-distance model for the nearest neighbors. The $P^+Q_A^-Q_B$ spectrum is very similar to that of the neutral dark state shown in Figure 2C.

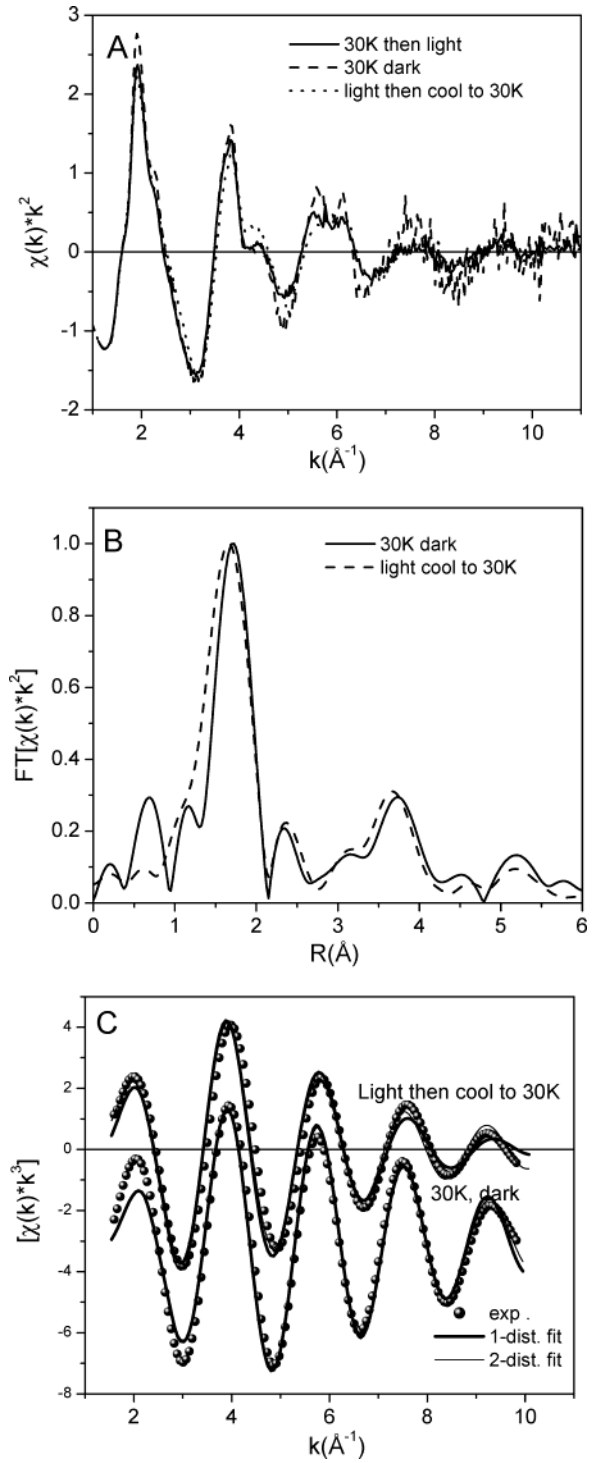

Figure 6. Mn K-edge XAFS spectra for Mn^{2+} site in Mn^{2+}–RC in neutral state PQ_AQ_B and charge separate state $P^+Q_AQ_B^-$ at 15 K. (A) k^2-weighted XAFS spectra; (B) FT-XAFS spectra (transformed from $k = 1.5-9.9$ Å^{-1}); (C) back-transformed XAFS spectra ($R = 0.92-2.17$ Å) for the first peak with fitting functions with one- and two-distance models.

are indeed sensitive to the structural changes in the protein matrix. The ultimate challenge is to correlate observed changes at the metal site to particular structural changes in the protein, which will be discussed in the following sections.

Temperature-Dependent Conformation Changes in the RC Proteins. The temperature dependence of kinetics in the electron-transfer reaction $P^+Q_A^-Q_B \rightarrow P^+Q_AQ_B^-$ and the charge recombination reactions $P^+Q_AQ_B^- \rightarrow PQ_AQ_B$ and $P^+Q_A^-Q_B \rightarrow PQ_AQ_B$ prompted extensive investigations on structural origins for these dynamic behaviors.[5−8,36] Structural differences between the X-ray diffraction studies on the dark-adapted ground state *Rb. sphaeroides* RC at 90 K and at room temperature shown in Figure 1A could be within the resolution of the technique, but significant and systematic differences in the nearest neighbor distances as well as distribution of the distant atoms from the

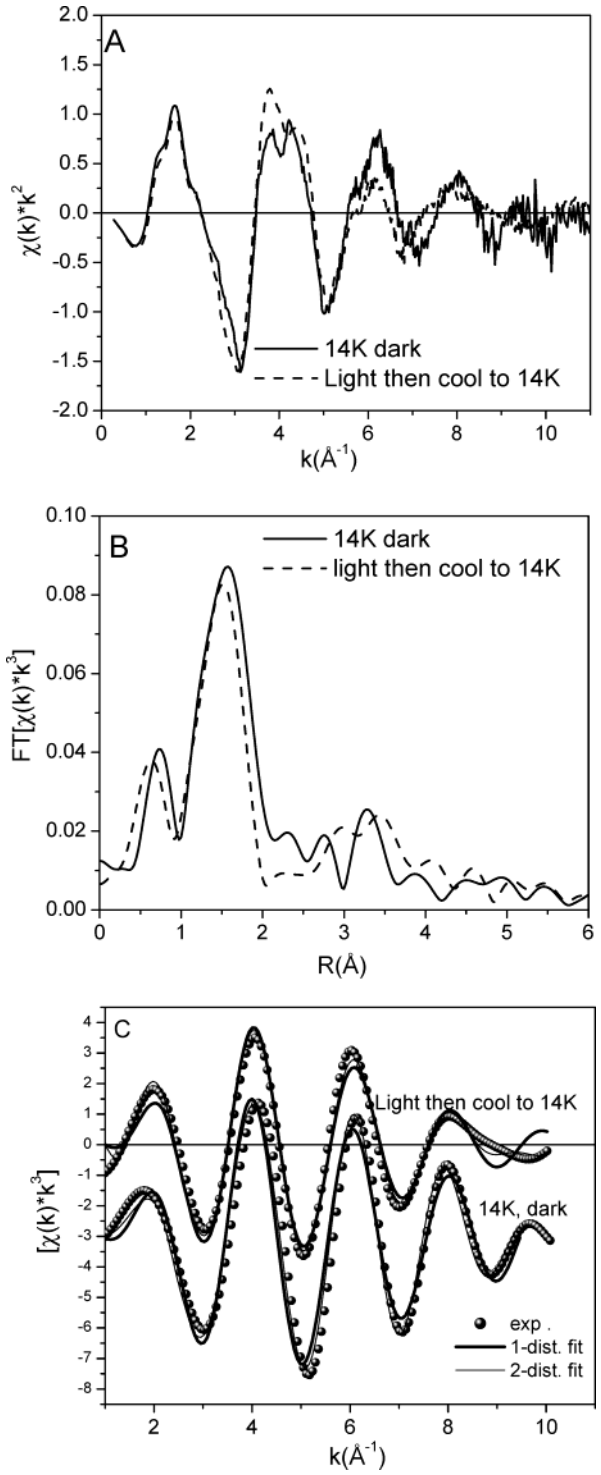

Figure 7. Zn K-edge XAFS spectra for Zn^{2+}−RC in neutral state PQ_AQ_B and charge separate state $P^+Q_AQ_B^-$ at 15 K. (A) k^2-weighted XAFS spectra; (B) FT-XAFS spectra (transformed from $k = 1.5-10.0$ $Å^{-1}$); (C) back-transformed XAFS spectra ($R = 1.0-2.1$ Å) for the first peak with fitting functions with one- and two-distance models.

Fe^{2+} are revealed by their XAFS spectra (Figure 1B). Our XAFS data on the Fe site inferred an average 0.04 Å Fe−N(O) bond expansion at cryogenic temperature, which is larger than the bond distance change in small Fe−N complexes under similar temperature changes in the absence of the spin state transition.[51] Therefore, the 0.04 Å Fe−N(O) expansion at low temperature is most likely an indication of protein structural changes imposed on the Fe site. In addition to the clear evidence for the central atom to the nearest neighbor bond expansion, an expansion in the second shell neighbors, corresponding to those C atoms connecting with N and O atoms coordinated with Fe^{2+}, was also observed. The expansion of the third shell is difficult to identify because of its broad distribution mainly from those atoms on the imidazole rings of His residue which are not directly connected to the Fe^{2+}.

The previous XAFS study on the RC proteins at room temperature and at 130 K observed no detectable difference in the Fe^{2+} site.[18] Such a result does not necessarily impose discrepancy between the two studies, because considerable structural changes between 130 and 15 K may occur, indicated by significant variation on the charge recombination rate between 18 and 113 K in a previous study.[3,36] The expansion of the Fe^{2+} to its neighboring atom distances at 15 K suggests a possible increase in average distance between Q_A and Q_B compared to that at room temperature. However, a previous study on the temperature dependence of the reaction rate for the charge recombination $P^+Q_A^-Q_B \rightarrow PQ_AQ_B$ process indicated possible contraction of the protein as temperature decreased, resulting in a stronger coupling between the electron donor and the acceptor, thus a faster reaction rate.[52] Our results for the low-temperature expansion of the protein matrix around the Fe^{2+} site do not contradict with this result, because the protein matrix expansion in the Q_A/Q_B region may occur concurrently with the contraction in the P/Q_A region. Nonetheless, the XAFS results cover the structural range up to the third atomic shell from the Fe^{2+}, the expansion of the Fe to ligand distance is an indication, but not a confirmation, of the protein matrix expansion in the region. According to Xu and Gunner,[15] the potential barrier for $P^+Q_A^-Q_B \rightarrow P^+Q_AQ_B^-$ reaction was about 340 meV or 23 kcal/mol, whereas the driving force for the reaction was less than 100 meV or less than 7 kcal/mol. Another study showed that the inner sphere reorganization energy for the Fe in cytochromes was about 8 kJ/mol or about 2 kcal/mol for one Fe−N bond to change the bond length by 0.03 Å,[53] which estimated the total inner reorganization energy for six Fe−N(O) bonds to change the bond length by the same amount to be about 15 kCal/mol. An ab initio quantum mechanical calculation on the metal binding energies with imidazole ligands obtained the stabilization energies due to the protein solvation and nonbonding interactions with neighboring residues to be about 34 and 55 kcal/mol, respectively.[54] Using these values to approximate the energetics around the Fe site of the RC, it is possible that the protein conformation change due to the lowering of the temperature should have sufficient driving force to lengthen the Fe−N(O) bond by 0.04 Å, as observed in the experiment.

The Charge Separation Induced Protein Structural Change—"Conformational Gating". It has been well-recognized that the structures of RC frozen in the dark and in the light to 70 K bear different conformations, the former prohibits the electron transfer from Q_A to Q_B, whereas the latter facilitates the reaction.[3,36] These two conformations have been referred to as the inactive and active conformations of the RC, respectively. At cryogenic temperature, the rate for the charge recombination reaction from the secondary quinine, $P^+Q_AQ_B^- \rightarrow PQ_AQ_B$ in the active conformation was almost the same as the room temperature, while the charge recombination from the primary quinone $P^+Q_A^-Q_B \rightarrow PQ_AQ_B$ was fourfold slower than at room temperature[3]. Although the X-ray diffraction studies on the RC identified the secondary quinone Q_B movement in the charge separation state $P^+Q_AQ_B^-$ compared to the ground-state PQ_AQ_B structure,[9] more studies have suggested that the conformational change in the surrounding protein matrix is not

only limited to the Q_B movement, but also protonation states as well as the configurations of the amino acid residues in the vicinity,[55−60] which may be too subtle to be resolved by the X-ray diffraction for the RC proteins.

With a much higher precision of the XAFS technique, we observed an average reduction of 0.04 Å in the Fe−N(O) distances in $P^+Q_AQ_B^-$ state from those of the PQ_AQ_B state at 15 K. According to the Stowell structure, the average distances from Q_A and Q_B to the Fe^{2+} are 8.9 and 11.6 Å, respectively, in the dark-adapted RC at 90 K, which presented an asymmetry of the two quinones relative to the Fe^{2+}. However, the corresponding light-adapted RC structure had an average Q_A to Fe^{2+} distance virtually unchanged while the average Q_B to Fe^{2+} distance reduced to 8.9 Å. Thus, the two quinone positions relative to the Fe^{2+} site is more symmetric in the charge separate state of $P^+Q_AQ_B^-$ than in the neutral state at 90 K. The fact that the one-distance model fits the Fe−N(O) bonds much better for the $P^+Q_AQ_B^-$ state than it does for the PQ_AQ_B state strongly suggests the change in the bond distance distribution.

Surprisingly, the Fe^{2+} site of PQ_AQ_B at 290 K also has a shorter average Fe−N(O) distance compared to that at 15 K, similar to that of the $P^+Q_AQ_B^-$ state trapped at 15 K. This observation is in accord with previous results where the $P^+Q_AQ_B^-$ state was only accessible when the initial illumination was at room temperature but was forbidden when it was cooled to cryogenic temperature in the dark.[3,36] The Fe^{2+} site XAFS spectrum of the RC frozen in the dark at 15 K clearly shows a different configuration from that of the room temperature and of the charge separate $P^+Q_AQ_B^-$ state. The cooling time from room temperature to 15 K in the dark took 30−40 min, which provided sufficient time for the RC protein to search for the minimum energy conformation at 15 K. Such a conformation was subsequently trapped and was unfavorable to perform the electron transfer from Q_A to Q_B.[3,36] The haut of the reaction was verified not only by optical spectroscopic measurements but also by the XAFS data in this study showing identical structures around the Fe^{2+} site at 15 K with and without the illumination (Table 1).

The similarity in the Fe^{2+} site structures at room temperature and charge-separated state $P^+Q_AQ_B^-$ revealed by the XAFS data could arise because of two reasons. First, several different conformations of the RC protein are populated in the dark, from which the conformation that facilitates the electron transfer from Q_A to Q_B is accessible at room temperature. As a result of dynamic averaging, the Fe−N(O) distances are shorter than those at 15 K. The differences among crystal structures from different samples at room temperature support such a scenario. Second, the Q_B could be reduced in the dark by X-ray at room temperature.[9] However, unless the reduction took place instantaneously after the sample was exposed to the X-ray, no change in XAFS spectra was observed with the data acquisition time to support such a hypothesis especially from the structural differences that were observed in the RC that was cooled in the dark from room temperature. Our results support that the conformation that facilitates the electron transfer is one of the energy minima of the RC protein at room temperature, but the results cannot rule out the structural herterogeneity from which the dynamic averaging of the structure results in a metal site with similar structural parameters as those of the charge separate state $P^+Q_AQ_B^-$. The charge separation state $P^+Q_AQ_B^-$ could change the energy landscape of the protein and may drive the protein conformation to stabilize the $P^+Q_AQ_B^-$ state. Because of difficulties in XAFS measurements at room temperature for the charge-separated state $P^+Q_AQ_B^-$ because of prolonged exposure to the light and X-ray, the structure of this state at room temperature was unavailable. Considering that five of the seven reported structures for wild type or spontaneous mutants of *Rb. sphaeriodes* RC placed Q_B in the proximal position and most of these structures were obtained at room temperature,[9,33−35,43,61−64] the structural similarity revealed at the Fe^{2+} site between the room temperature in the neutral state and cryogenic temperature in $P^+Q_AQ_B^-$ state supports or reconfirms the X-ray diffraction results on a local structure level with much higher precision. In addition, recent X-ray scattering results on the RC protein at room temperature obtained in both the dark and the light (Tiede, unpublished results) could not detect structural difference between the two states, which is agreeable with the XAFS results.

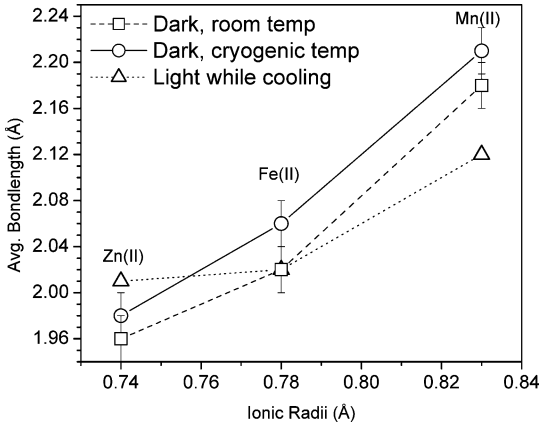

Figure 8. The average nearest neighbor bond distance from two-distance fits as listed in Tables 1−3 vs ionic radii of the metal ions obtained from XAFS data analyses.

Effects of Metal Replacement on the RC Structure and Their Implications. The role of the Fe^{2+} site in the RC protein function as transporting electrons across the membrane has been examined extensively in the past by kinetics measurements on the electron-transfer rate in the RC with various modifications relevant to the Fe^{2+} site, such as removal of the Fe^{2+} or replacing it with other divalent metal ions.[37,46,49] The removal of the Fe^{2+} was known to alter the protein integrity and destabilize the protein, which affected the kinetics of the electron transfer.[46] Replacing the Fe^{2+} with other divalent metal ions maintained the kinetics of the electron transfer on 100 μs time scale.[46] However, the XAFS results in the RC with Fe^{2+} replaced by Mn^{2+} and Zn^{2+} show that the local structures have been altered by the metal ion replacement. Similarly, structural changes in these metal ion replaced RC proteins could be driven by either temperature change or the $P^+Q_AQ_B^-$ state formation induced by light as in the Fe^{2+}−R26−RC, but the amount of structural changes vary with the metal. Apparently, at a certain temperature or at the charge-separated state $P^+Q_AQ_B^-$, the average nearest neighbor distances from the divalent metal ions in the RC are strongly correlated with ionic radii as shown in Figure 8. Such a relationship indicates the adaptability of the protein environment around the metal sites, where amino acids are capable of accommodating metal ions of different sizes. On the other hand, the metal ion in the Fe^{2+} site is able to pull or push the surrounding amino acids around to meet its need for the optimal coordination with its neighbors. Consequently, the protein matrix in the vicinity and the kinetics for the electron-transfer reaction in the Q_A/Q_B region may be altered by the way metal ion binds.

Despite the fact that both Mn^{2+} and Zn^{2+} substituted RC protein are capable of carrying out the electron transfer from

Q_A to Q_B,[8,46] their structural responses to the temperature change and the formation of $P^+Q_AQ_B^-$ state are not necessarily the same as the Fe^{2+} site in unmodified RC protein. Figure 8 shows a general trend for the average nearest neighbor distance change around the metal ion because of the temperature change, as well as because of the formation of the charge separation state $P^+Q_AQ_B^-$. Although the origins of these trends are not completely clear, some metal dependent behaviors can be rationalized on the basis of size and electronic structure of these metal ions. The crystal field stabilization energy for Mn^{2+} ($3d^5$, high spin) or Zn^{2+} ($3d^{10}$) in an ideal octahedral coordination site with all identical ligands is zero, whereas that for Fe^{2+} ($3d^6$, high spin) is positive, having stronger Fe−ligand bonds than the other two metal ions.[65] This was seen in crystal structures of corresponding metal oxalate dihydrates, where the Fe−O distances were the shortest.[41,42] Apparently, the crystal field stabilization energy could not compete with the potential barriers imposed by the stereo hindrance by the protein matrix. According to the XAFS results (Table 2), structural changes due to the formation of $P^+Q_AQ_B^-$ state are larger in Mn^{2+}−RC than those in Fe^{2+}−RC. With a radius of 0.83 Å, 0.05 Å larger than that of Fe^{2+}, Mn^{2+} could impose a tighter packing in the protein and pushes the coordinated amino acids away. The significantly lower magnitude for the second peak in the FT-XAFS spectra of Mn^{2+}−RC (Figure 6B) suggests that the alignment of the second shell atoms with the nearest neighbors and the metal, and thus the coordination geometry of the ligands, was disturbed by the Mn^{2+} replacement. Consequently, the protein vicinity and the relative distance and the orientation of $Q_{A,B}$ could be disturbed as well. However, the local structural changes due to the temperature around Mn^{2+} do not behave differently from those around the Fe^{2+} site, which may be an indication that conformation changes caused by temperature and the light-induced charge separation follow different paths in the energy landscape of the RC protein.

On the other hand, replacing Zn^{2+} with a radius of 0.74 Å, 0.04 Å smaller than Fe^{2+}, may result in a more flexible protein matrix that allows the ligands to be pulled toward the Zn^{2+}, resulting in smaller average Zn−N(O) distances than Fe−N(O) distances. Compared to Fe^{2+} and Mn^{2+} sites where overall peak shapes and intensities under different conditions were largely reserved, the XAFS spectra of Zn^{2+} vary more considerably in their overall peak shapes and intensities, especially for distant atomic shells. Such an observation implies more variations in the Zn^{2+} site structures because of temperature change and the light-induced charge separation, even when the nearest neighbor distances did not change significantly. It is also possible that the Fe removal and Zn replacement were carried out by chaotropic procedures that loosened the protein matrix, whereas the replacement of Mn^{2+} was carried out biosynthetically to yield a protein better retained to its native state.

The XAFS spectra of the metal sites revealed at least three causes that alter the protein energy landscape in the vicinity of the Fe^{2+} site in RC proteins: (1) temperature change, (2) protein packing change due to the metal ion binding, and (3) charge distribution change due to the formation of $P^+Q_AQ_B^-$ state. The temperature change alters statistically averaged populations of RC proteins in PQ_AQ_B state with different conformations related to energy minima in the protein energy landscape as well as the interconversion rates between different conformations. The metal replacement in the formal Fe^{2+} site alters the shape of the potential surface and the conformations that correspond to energy minima. The charge redistribution due to the formation of $P^+Q_AQ_B^-$ state can alter the potential barriers in different ways that may open the path on the potential energy landscape for the protein to reach the conformation that facilitates the charge separation.

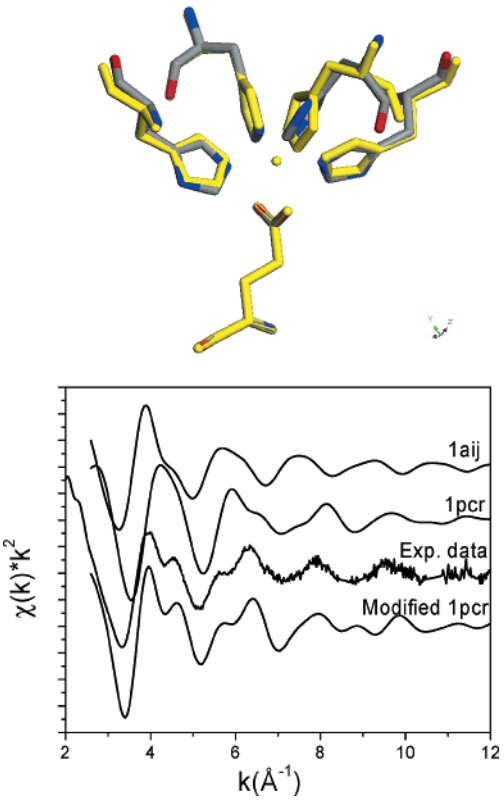

Figure 9. XAFS spectra of Fe site from 1*aij*, 1*pcr* (yellow), experimental data, and modified 1*pcr* (colored).

Implications of Fe Site Structures of RC from XAFS Results. Apparently, none of the Fe site structure generated good agreement with the XAFS data after examining several RC structures with the highest available resolution, which implies significant discrepancy between the actual Fe site structures and crystallographic data. We are inspired by a recent publication by Hasnain and Strange, in which they showed that even structures of metalloproteins with resolution as high as 1.9 Å still generated XAFS spectra significantly different from experimental XAFS data whereas those for the metal binding sites from crystallographic data with 0.9 Å resolution agreed well with the XAFS data. Thus, it is not surprising that the RC structure with 2.2 or 2.6 Å resolution could not agree with our XAFS data. We have attempted modifications in local coordination environments of Fe from the 1*pcr* coordinates to match the experimental XAFS data. One of the modifications shows a significant improvement in terms of the agreement with the experimental data as shown in Figure 9. The modification was made by varying orientations of four imidazole rings of His residues relative to the Fe in such a way that distances of the second and third shell atoms from Fe^{2+} are more homogeneous than in the original 1*pcr* structure.[43] Such modification at this stage is for demonstration purposes only and hence ignores the consequences to the protein backbone, which only includes the disconnected His residues from the protein backbone. However, this initial attempt of structure−spectrum matching demonstrates that the actual Fe site structure in the RC could significantly deviate from currently available crystallographic data in terms of ligand orientation and distance. Therefore, XAFS results can provide information on the correctness of the diffraction data and may shed light on which structural adjustment is required

to get better resolution around metal site. Our study indicated that significant adjustment on the Fe site structure of the RC from current coordinates from the diffraction data is required.

Summary

Subtle structural changes around the Fe^{2+} site in the bacterial photosynthetic reaction center protein have been detected by the metal K-edge XAFS spectra. These changes occur in response to lowering temperature, the formation of the charge-separated state $P^+Q_AQ_B^-$, and the replacement of the Fe^{2+} with other divalent metal ions. Evidence for protein expansion in the dark near the Fe^{2+} site at 15 K from that at room temperature has been obtained and can be used to rationalize the exclusion of $P^+Q_AQ_B^-$ state at cryogenic temperature. Different structural responses at the metal site due to temperature change and charge separation suggest that these conformation changes are cause dependent. On the basis of the XAFS results for the RC proteins with different divalent metal ions replacement at the formal Fe^{2+} site, a correlation between average metal−N(O) bond lengths as a function of metal ionic radii is established. Minor adjustments of the imidazole rings of His residuals to a more symmetric orientation with respect to the Fe^{2+} significantly improves the agreement between the calculated and experimental XAFS spectra, demonstrating the sensitivity of XAFS spectra to the structural changes that could be overlooked by the diffraction data, and the potential of using XAFS spectra to refine the metal site structure in proteins. Further experimentation involving kinetic measurements of metal-replaced RCs is being planned to correlate the local structures around metal ion sites to the electron-transfer function.

Acknowledgment. This work is supported by the Division of Chemical Sciences, Office of Basic Energy Sciences, U.S. Department of Energy under contracts W-31-109-Eng-38. The authors wish to thank Drs. S. S. Hasnain and R. W. Strange for providing coordinates for the Cu sites in several proteins they have studied, which helped us to understand the Fe site structure in the RC. Technical assistance from M. Beno, J. Linton, and staff members at BESSRC-CAT, Advanced Photon Source, is greatly appreciated.

Abbreviations: RC, reaction center; XAFS, X-ray absorption fine structure; EPR, electron paramagnetic resonance; P, special pair bacterial chlorophylls; Q_A, primary quinine; Q_B, secondary quinine; His, histidine; Glu, glutamic acid

References and Notes

(1) Wang, Z.; Pearlstein, R. M.; Jia, Y.; Fleming, G. R.; Norris, J. R. *Chem. Phys.* **1993**, *176*, 421.
(2) Parson, W. W.; Chu, Z. T.; Warshel, A. *Biophys. J.* **1998**, *74*, 182.
(3) Kleinfeld, D.; Okamura, M. Y.; Feher, G. *Biochim. Biophys. Acta* **1984**, *766*, 126.
(4) McPherson, P. H.; Okamura, M. Y.; Feher, G. *Biochim. Biophys. Acta* **1990**, *1016*, 289.
(5) Tiede, D. M.; Vazquez, J.; Cordova, J.; Marone, P. A. *Biochemistry* **1996**, *35*, 10763.
(6) Li, J.; Gilroy, D.; Tiede, D. M.; Gunner, M. R. *Biochemistry* **1998**, *37*, 2818.
(7) Graige, M. S.; Feher, G.; Okamura, M. Y. *Proc. Natl. Acad. Sci. U.S.A.* **1998**, *95*, 11679.
(8) Utschig, L. M.; Ohigashi, Y.; Thurnauer, M. C.; Tiede, D. M. *Biochemistry* **1998**, *37*, 8278.
(9) Stowell, M. H. B.; McPhillips, T. M.; Rees, D. C.; Solitis, S. M.; Abresch, E.; Feher, G. *Science* **1997**, *276*, 812.
(10) Fritzsch, G.; Koepke, J.; Diem, R.; Kuglstatter, A.; Baciou, L. *Acta Crystallogr.* **2002**, *D58*, 1660.
(11) Xu, Q.; Baciou, L.; Sebban, P.; Gunner, M. R. *Biochemistry* **2002**, *41*, 10021.
(12) Breton, J.; Buollais, C.; Mioskowski, C.; Sebban, P.; Baciou, L.; Nabedryk, E. *Biochemistry* **2002**, *41*, 12921.
(13) Lavergne, J.; Matthews, C.; Ginet, N. *Biochemistry* **1999**, *38*, 4542.
(14) Xu, Q.; Gunner, M. R. *Biochemistry* **2002**, *41*, 2694.
(15) Xu, Q.; Gunner, M. R. *Biochemistry* **2001**, *40*, 3232.
(16) Schmid, R.; Labahn, A. *J. Phys. Chem. B* **2000**, *104*, 2928.
(17) Mezzetti, A.; Nabedryk, E.; Breton, J.; Okamura, M. Y.; Paddock, M. L.; Giacometti, G.; Leibl, W. B. *Biochim. Biophys. Acta* **2002**, *1553*, 320.
(18) Eisenberger, P.; Okamura, M. Y.; Feher, G. *Biophys. J.* **1982**, *37*, 523.
(19) Bunker, G.; Stern, E. A.; Blankenship, R. E.; Parson, W. W. *Biophys. J.* **1982**, *37*, 539.
(20) Feher, G.; Okamura, M. Y. *Appl. Magn. Reson.* **1999**, *16*, 63.
(21) Sayers, D. E.; Stern, E. A.; Lytle, F. *Phys. Rev. Lett.* **1971**, *27*, 1204.
(22) Stern, E. A.; Sayers, D. E.; Lytle, F. W. *Phys. Rev. B* **1975**, *11*, 4836.
(23) Lytle, F. W.; Sayers, D. E.; Stern, E. A. *Phys. Rev. B* **1975**, *11*, 4825.
(24) Hasnain, S. S.; Strange, R. W. *J. Synchrotron Radiation* **2003**, *10*, 9.
(25) Hasnain, S. S.; Hodgson, K. O. *J. Synchrotron Radiation* **1999**, *6*, 852.
(26) Dimakis, N.; Bunker, G. *Phys. Rev. B: Condens. Matter* **2002**, *65*, 201103/1.
(27) Kleifeld, O.; Kotra, L. P.; Gervasi, D. C.; Brown, S.; Bernardo, M. M.; Fridman, R.; Mobashery, S.; Sagi, I. *J. Biol. Chem.* **2001**, *276*, 17125.
(28) Glaser, T.; Hedman, B.; Hodgson, K. O.; Solomon, E. I. *Acc. Chem. Res.* **2000**, *33*, 859.
(29) Bianconi, A.; Natali, F.; Alosi, M. L.; Grande, S.; Lanzara, A.; Saini, N. L.; Brunelli, M. *J. Synchrotron Radiation* **1999**, *6*, 389.
(30) Powers, L.; Griep, M. A. *Biochemistry* **1999**, *38*, 7413.
(31) Yachandra, V. K. *Methods Enzymol.* **1995**, *246*, 638.
(32) Allen, J. P.; Feher, G.; Yeates, T. O.; Rees, D. C.; Deisenhofer, J.; Michel, H.; Huber, R. *Proc. Natl. Acad. Sci. U.S.A.* **1986**, *83*, 8589.
(33) Allen, J. P.; Feher, G.; Yeates, T. O.; Komiya, H.; Rees, D. C. *Proc. Natl. Acad. Sci. U.S.A.* **1987**, *84*, 5730.
(34) Allen, J. P.; Feher, G.; Yeates, T. O.; Komiya, H.; Rees, D. C. *Proc. Natl. Acad. Sci. U.S.A.* **1988**, *85*, 8487.
(35) Chang, C. H.; el-Kabbani, O.; Tiede, D.; Norris, J.; Schiffer, M. *Biochemistry* **1991**, *30*, 5352.
(36) Kleinfeld, D.; Okamura, M. Y.; Feher, G. *Biochemistry* **1984**, *23*, 5780.
(37) Utschig, L. M.; Greenfield, S. R.; Tang, J.; Liable, P. D.; Thurnauer, M. C. *Biochemistry* **1997**, *36*, 8548.
(38) Utschig, L. M.; Poluektov, O.; Tiede, D. M.; Thurnauer, M. C. *Biochemistry* **2000**, *39*, 2961.
(39) Straley, S. C.; Parson, W. W.; Mauserall, D. C.; Clayton, R. K. *Biochim. Biophys. Acta* **1973**, *305*, 597.
(40) Jennings, G.; Jaeger, W. J. H.; Chen, L. X. *Rev. Sci. Instrum.* **2002**, *72*, 362.
(41) Deyreux, R.; Barro, C.; Peneloux, A. *Bull. Soc. Chim. Fr.* **1973**, 25.
(42) Sharov, V. A. *Russ. J. Inorg. Chem.* **1977**, *22*, 1500.
(43) Ermler, U.; Fritzsch, G.; Buchanan, S. K.; Michel, H. *Structure (London)* **1994**, *2*, 925.
(44) Holm, R. H.; Kennepohl, P.; Solomon, E. *Chem. Rev.* **1996**, *96*, 2239.
(45) Poleuktov, O. G.; Utschig, L. M. Unpublished results.
(46) Debus, R. J.; Feher, G.; Okamura, M. Y. *Biochemistry* **1986**, *25*, 2276.
(47) Sigel, A.; Sigel, H. *Probing Proteins by Metal Ions and Their Low-Molecular-Weight Complexes;* Marcel Dekker: New York, 2001; Vol. 38.
(48) Blankenship, R. E.; Parson, W. W. *Biochim. Biophys. Acta* **1979**, *545*, 429.
(49) Kirmaier, C.; Holten, D.; Debus, R. J.; Feher, G.; Okamura, M. Y. *Proc. Natl. Acad. Sci. U.S.A.* **1986**, *83*, 6407.
(50) Chen, L. X.; Bowman, M. K.; Montano, P. A.; Norris, J. R. *Mater. Res. Soc. Symp. Proc.* **1993**, *307*, 45.
(51) Chen, L. X.; Wang, Z.; Burdett, J. K.; Montano, P. A.; Norris, J. R. *J. Phys. Chem.* **1995**, *99*, 7958.
(52) Ortega, J. M.; Mathis, P.; Williams, J. C.; Allen, J. P. *Biochemistry* **1996**, *35*, 3354.
(53) Sigfridsson, E.; Olsson, M. H. M.; Ryde, U. *J. Phys. Chem. B* **2001**, *105*, 5546.
(54) Peschke, M.; Blades, A. T.; Kebarle, P. *J. Am. Chem. Soc.* **2000**, *122*, 1492.
(55) Zachariae, U.; Lancaster, C. R. D. *Biochim. Biophys. Acta* **2001**, 1.
(56) Peluso, A.; Donato, M. D.; Saracino, G. A. A. *J. Chem. Phys.* **2000**, *113*, 3212.

(57) Walden, S. E.; Wheeler, R. A. *J. Phys. Chem. B* **2002**, *106*, 3001.
(58) Kuglstatter, A.; Ermler, U.; Michel, H.; Baciou, L.; Fritzsch, G. *Biochemistry* **2001**, *40*, 4253.
(59) Tandori, J.; Maroti, P.; Alexov, E.; Sebban, P.; Baciou, L. *Proc. Natl. Acad. Sci. U.S.A.* **2002**, *99*, 6702.
(60) Tandori, J.; Baciou, L.; Alexov, E.; Maroti, P.; Schiffer, M.; Hanson, D. K.; Sebban, P. *J. Biol. Chem.* **2001**, *276*, 45513.
(61) Komiya, H.; Yeates, T. O.; Rees, D. C.; Allen, J. P.; Feher, G. *Proc. Natl. Acad. Sci. U.S.A.* **1988**, *85*, 9012.
(62) Feher, G.; Allen, J. P.; Okamura, M. Y.; Rees, D. C. *Nature (London)* **1989**, *339*, 111.
(63) El-Kabbani, O.; Chang, C. H.; Tiede, D.; Norris, J.; Schiffer, M. *Biochemistry* **1991**, *30*, 5361.
(64) Rees, D. C.; Chirino, A. J.; Kim, K. H.; Komiya, H. *Membrane protein structure and stability: Implications of the first crystallographic analyses* 1994; Vol. 1.
(65) Percy, G. C.; Thornton, D. A. *J. Mol. Struct.* **1971**, *10*, 39.